Numerical Evaluation of Long-Term Depressurization Production of a Multilayer Gas Hydrate Reservoir and Its Hydraulic Fracturing Applications

Lv, Tao; Cai, Jing; Ding, Yalong; Pan, Jie; Chen, Zhaoyang; Li, Xiaosen

Published in:
Energy and Fuels

Link to article, DOI:
10.1021/acs.energyfuels.1c04017

Publication date:
2022

Document Version
Peer reviewed version

Numerical evaluation of long-term depressurization production of multilayer gas hydrate reservoir and its hydraulic fracturing application

Tao Lv[a,b,*], Jing Cai[b,c,d], Yalong Ding[e], Jie Pan[a], Zhaoyang Chen[b,c], Xiaosen Li[b,c]

[a] *College of petroleum engineering, Xi'an Shiyou University, Xi'an 710065, PR China*

[b] *Key Laboratory of Gas Hydrate, Guangzhou Institute of Energy Conversion, Chinese Academy of Sciences, Guangzhou 510640, PR China*

[c] *Guangdong Provincial Key Laboratory of New and Renewable Energy Research and Development, Guangzhou 510640, PR China*

[d] *Center for Energy Resources Engineering, Department of Chemical and Biochemical Engineering, Technical University of Denmark, Lyngby 2800 Kgs., Denmark*

[e] *College of Chemistry and Pharmaceutical Engineering, Huanghuai University, Zhumadian 463000, PR China*

ABSTRACT

In this study, a multilayer gas hydrate reservoir (hydrate, gas and water) model was implemented based on the geological conditions of Shenhu Area in the South China Sea (SHCS), to predict the production performance of the reservoir during long-term depressurization. Hydraulic fracturing technology was introduced to boost production, and its positive and negative impacts on the production behaviors of hydrate reservoir was evaluated respectively. Results show that the hydrate dissociation is severely constrained by pressure propagation and fluids flow in the low reservoir. During production, almost half of wellhead gas production is from the dissolved gas in seawater and the free gas contained in sediments. Massive secondary hydrate forms and gathers near the bottom of the dissociation front and the interface of hydrate layers. Underlying free gas is conducive to reservoir production, in which the cumulative wellhead gas production can be increased by ~59% compared to the reservoir lacking underlying free gas. On one hand, hydraulic fracturing can significantly promote hydrate dissociation and increase the capacity of production, especially for long-distance fracture implemented in the middle part of hydrate layer.

On the other hand, the high permeability in fractured zone also provides a convenient channel for water in the sedimentary layer. After hydraulic fracturing, the production efficiency of the reservoir is still low due to the involvement of more pore water. In future, the combination of hydraulic fracturing and other auxiliary means can be considered to develop the hydrate reservoirs.

KEYWORDS

Gas hydrate, multilayer reservoir, low permeability, underlying free gas, hydraulic fracturing, secondary hydrate

1. INTRODUCTION

Gas hydrate is an ice-like crystal formed by water molecules and hydrocarbon (mainly methane) molecules under suitable pressure and temperature conditions.[1,2] In nature, gas hydrate is generally observed in the regions of deep-sea sediments and offshore continental margins.[3] The amount of hydrate-bound methane is estimated to be 10^{15}~10^{18} ST m^3, of which the amount of technically recoverable methane is up to 10^{14} ST m^3.[4] To date, more than 220 potential reservoir sites were discovered.[5] Gas hydrate is widely considered a potential energy resource, which will change the future energy structure and play an important role in it. The vigorous development and utilization of hydrate resources can promote the global green and low-carbon economy, but how to effectively extract gas from the reservoirs is a challenge.

The gas extraction methods mainly include depressurization, thermal stimulation, CO_2 replacement, chemical reagent injection and their combinations.[6-10] Among them, depressurization is recognized as one of the most promising methods due to its simple implementation,[6] and has been applied in multiple on-site trial tests (Table 1), including 6 times in marine hydrate reservoirs. Especially, the representative projects are the tests conducted in the Nankai Trough, Japan (2013) and the Shenhu Area, China (2017 and 2020). In addition, massive research on specific depressurization parameters, such as rate, amplitude and strategy, etc., were carried out in laboratory. Feng et al.[11] experimentally investigated the effect of depressurization rate on methane hydrate dissociation and deduced there exists an optimal rate during production. Li et al.[12] indicated the production behavoirs of the hydrate reservoir is

closely related to the depressurization amplitude. Although reducing the production pressure could increase the amount of gas production, it also leads to a remarkable increase in cumulative water production. Merey et al.[13] evaluated the effect of depressurization amplitude on the production performance of hydrate reservoir in the Black Sea. Meanwhile, the reasonable depressurization operation could reduce sand and water output at wellhead. Phillips et al.[14] indicated that the stepwise depressurization strategy helps to reduce wellhead water production, but has little contribution to the overall gas production. Lv et al.[15,16] investigated the one-step rapid and stepwise depressurization strategies on laboratory-scale hydrate reservoirs. The results showed that the stepwise depressurization can alleviate the heat loss and sand production of the reservoir, and which possess a stable gas recovery process. Gao et al.[17] found that the implementation of stepwise depressurization strategy for hydrate production can control the cumulative water production at wellhead in each stage, and improve the overall energy efficiency ratio. Besides, Konno et al.[18] proposed a cyclic depressurization method in an attempt to achieve the sustainable production of hydrate reservoirs. Wu et al.[19] simulated the gas production process of hydrate reservoir in the Nankai Trough and investigated the effect of well pattern layout on the reservoir production. To explore the synergistic interactions between production wells, multiple wells combined depressurization to produce gas from hydrate reservoirs were also investigated by numerical analysis and simulation.[20,21]

Actually, the exploitation of field hydrate reservoir involves the process of hydrate formation and dissociation, gas/liquids/solids multiphase seepage and heat transfer, etc. Especially for the Class I hydrate reservoir, the existence of underlying free gas could aggravate the phase change, fluids flow and heat transfer in the reservoir. The coexistence of gas hydrate, free gas and water in the hydrate system has been identified in several sites, including the Shenhu Area,[25] the Sanriku-Oki Forearc Basin,[26] the Mannar Basin[27] and the Hikurangi Margin.[28] Therefore, it is very necessary to understand the role of free gas during hydrate reservoir production. Through experiments, Yang et al.[29] found that hydrate dissociation rate and the cumulative gas/water production are positively correlated with the pressure of

underlying free gas layer. Lu et al.[30] indicated that the contribution of underlying free gas to production is mainly concentrated in the initial stage. Song et al.[31] compared the production behaviors of hydrate reservoirs with excess gas and excess water by using MRI imaging technology. The results demonstrated that for the former, the hydrate preferentially dissociates along the peripheries of samples, and for the latter, the hydrate dissociation process is more uniform. Nevertheless, during long-term production of the hydrate reservoirs, the impacts of the underlying free gas is still not clear enough.

Table 1 Test production results of global gas hydrate reservoirs[14,22-24]

Region	Reservoir characteristics	Year	Method	Duration time	Gas production/ ST m^3
Messoyakha	Gravel layer k = 125 mD S_H = 40% φ = 16%~38%	1972-1989	Depressurization/chemical reagent	Intermittent production for 17 years	36% from hydrate
Mallik site	Gravel layer S_H = 47% φ = 29.3%	2002	Hot brine/Depressurization	125h	516
		2007	Depressurization/thermal stimulation	12.5h	830
		2008	Depressurization	139h	13,000
Ignik Sikumi	Gravel layer k =1700 mD S_H = 60~75% φ = 40%	2012	CO_2 replacement CO_2/N_2 (23/77%)	~6w	24,085
Nankai Trough	Coarse sand S_H = 60% k =1 D	2013	Depressurization	6d	119,500
		2017(1)	Depressurization	12d	35,000
		2017(2)	Depressurization	24d	240,000
Shenhu Area	Clay-silty sand k = 0.2~20 mD S_H = 30~50% φ = 33%	2017	Depressurization	60d	309,000
		2017	Solid fluidization	-	81
		2020	Depressurization	30d	861,400

In addition, gas hydrate always exists in fine-grained sediments with a relatively low intrinsic permeability, that is, the resources are low-grade.[32] For developing such reservoirs, the urgent problem is to break the restriction of permeability on the pressure propagation and fluids flow in the reservoir, so as to improve the capacity of production.[33] According to the exploitation experience of traditional oil and gas reservoirs, hydraulic fracturing is usually an effective measure to reform reservoirs

and boost production.[34] Previously, Too et al.[35] conducted fracturing tests in highly saturated hydrate sediments and realized artificial cracks using hydraulic fracturing. Liu et al.[36] verified the feasibility of hydraulic fracturing in hydrate-bearing sediments by using the analytic hierarchy process-entropy method. Zhao et al.[37] testified that the enhancing effect of hydraulic fracturing on hydrate reservoir production through experiments, and found that the high permeability of fractured zone can promote the fluids flow in reservoir and wellhead gas production. The results of numerical simulation also showed that in the early stage, the average gas production rate of hydrate reservoir can be significantly improved after hydraulic fracturing.[38,39] Similarly, Zhang et al.[40] creatively introduced an artificial enlarged well wall into the exploitation of hydrate reservoirs. The studies mentioned above all confirmed the feasibility and effectiveness of hydraulic fracturing for hydrate reservoir production. Furthermore, the specific fracturing parameters, especially the effect of fracture depth and fracture length on production performance of hydrate reservoirs, need to be fully evaluated.

In this study, a multilayer hydrate reservoir model with the coexistence of hydrate, free gas and water was established based on the geological conditions of SCHS. By using TOUGH + HYDRATE, we predicted the production performance of the reservoir during a 10-year depressurization period and evaluated the effect of underlying free gas on hydrate dissociation, gas and water production behavoirs. Moreover, hydraulic fracturing was introduced in the production process of hydrate reservoir, and how the fracture depth and fracture length affect the process was analyzed, respectively. It is sincerely hoped that these results can provide some references for the practical production of hydrate reservoirs.

2. METHOD

2.1 Reservoir Characteristics

The Shenhu Area locates between the Xisha Trough and Dongsha Islands in the Northland of the South China Sea and is the intersection of the Eurasian plate, the Pacific plate, and the Indian-Australian plate. The strata in this area not only possesses excellent channels for hydrocarbon gas migrating but has suitable

temperatures and pressures to form hydrate.[41] It was predicted that the amount of hydrate-bound methane in this area is about 1.6×10^{10} ST m^3.[23] In the stratum, the ground temperature gradient is between 0.043 K/m and 0.068 K/m, and the average seafloor heat flow is about 76 mW/m^2. The salinity of pore water is between 2.90 wt% ~ 3.15 wt%. Distinctively, the sediments of the reservoir are mainly silty sand (32-63 μm) with a clay content of not less than 20 %, resulting in an extremely low permeability in sedimentary layers, which also poses a great challenge to extract gas from the hydrate reservoir. In this study, the simulated area is located at station W17 (the site of the first field test) in the SHCS, the seawater depth is 1266 m, and the hydrate layer is located 200~250 m below the seabed. According to the exploration data, the reservoir belongs to the Class I type, which can be divided into two hydrate layers and an underlying free gas layer.[25,42]

2.2 Model Description, Domain Discretization, and Production Scheme

Figure 1(a) shows the established hydrate reservoir model (cylinder model) in this study. The simulation domain along the vertical direction (Z) is 477 m, where the thickness of hydrate layer I, hydrate layer II and mud layer (underlying free gas layer) is 35 m (-235 m $\leq Z \leq$ -200 m), 15 m (-250 m $\leq Z \leq$ -235 m), and 27 m (-277 m $\leq Z \leq$ -250 m), respectively. The overburden with a thickness of 200 m (-200 m $\leq Z \leq$ 0 m), is extended up to the seabed. After several calculation trials, the thickness of underburden is also extended to 200 m (-477 m $\leq Z \leq$ -277 m), which is sufficient to describe the heat flow exchange between adjacent layers because of the low intrinsic permeability.[7] The radial value (R) of the simulation domain is 150 m, and its outermost side is regarded as a flowing boundary. The relevant parameters, such as saturation, porosity, permeability and formation conditions are all consistent with the reported parameters, as listed in Table 2.

The cylindrical system is discretized to $81 \times 194 = 15714$ grids along with the R and Z directions. The top and bottom boundaries of the simulation domain are defined as inactive grids, and their temperatures and pressures remain constant during production. Along Z direction, the overburden/underburden is respectively divided into 20 grids according to the principle of arithmetic sequence growth and equidistant,

and the specific division can be seen in Figure 1(b). The hydrate layer I, II, and mud layer is evenly divided into 70, 30, and 54 grids with a spacing of 0.5 m, respectively. Along *R* direction, the model is divided into 81 grids according to the principle of logarithmic growth, where the initial grid length is 0.05 m.

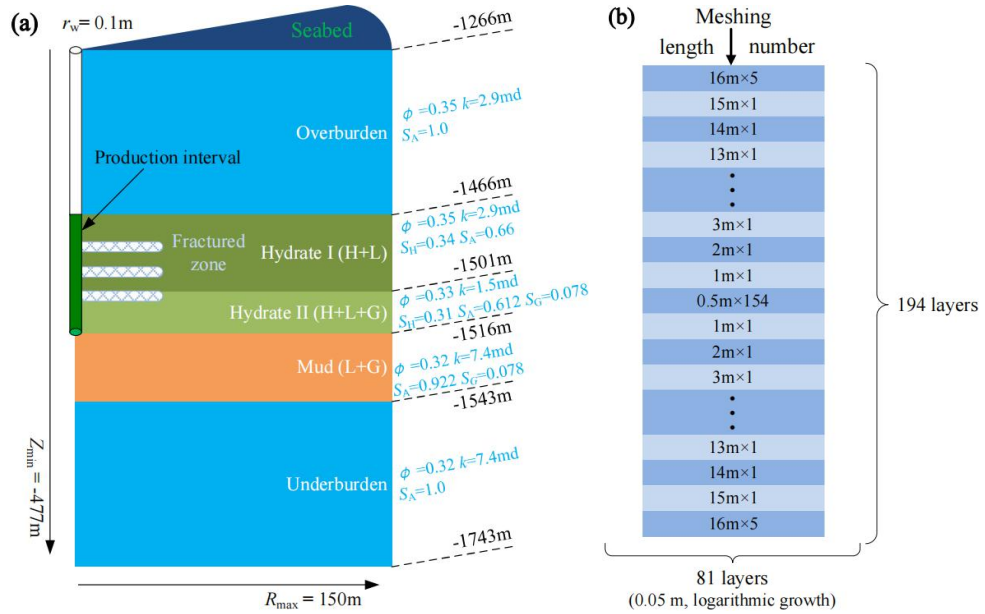

Figure 1 Diagrammatic sketch of the established model (a) and meshing (b) at station W17

Table 2 Physical parameters and formation conditions of the reservoir model

Parameters	Value
Overburden	200 m
Underburden	200 m
Hydrate layer I	35 m
Hydrate layer II	15 m
Mud layer	27 m
Initial P_B (Bottom of hydrate layer II)	15.521 MPa
Initial T_B (Bottom of hydrate layer II)	14.93 °C
Gas composition	100% CH_4
Geothermal gradient	0.0443 K/m
Salinity of pore water	3.05%
Permeability in production well	1000 D
Permeability of fractured zone	1000 mD
Sediment density	2200 kg/m^3
Wet thermal conductivity $k_{\Theta RW}$	1.7 W/m/K
Dry thermal conductivity $k_{\Theta RD}$	1.0 W/m/K
Composite thermal conductivity model[43,44]	$k_{\Theta C} = k_{\Theta RD}+(S_A^{1/2}+S_H^{1/2})(k_{\Theta RW} - k_{\Theta RD})+\phi S_I\, k_{\Theta I}$
Capillary pressure model[45]	$P_{cap} = - P_{0l}[(S^*)^{-1/\lambda} - 1]^{1-\lambda}$ $S^* = (S_A - S_{irA})/(S_{mxA} - S_{irA})$
S_{irA}	0.30

λ	0.45
P_{01}	10^5 Pa
Relative Permeability Model[43,46]	$k_{Ra} = (S_A^*)^n$, $k_{rG} = (S_G^*)^{nG}$ $S_A^* = (S_A - S_{irA})/(1 - S_{irA})$ $S_G^* = (S_G - S_{irG})/(1 - S_{irA})$
n	5.00
n_G	3.50
S_{irG}	0.03

The production well is a single vertical well located at the center of the cylinder with an effective radius of 0.1 m, as shown in Figure 1(a). In the reservoir, hydrate layer II is closely connected with hydrate layer I, and which is a mixed layer with coexistence of hydrate, free water and free gas, indicating that its formation temperatures and pressures are close to the hydrate phase equilibrium conditions. Therefore, it is necessary to product them together, that is, the production interval (35 m) is simultaneously penetrated hydrate layers I and II. The pressure of production well is maintained at 4.5 MPa, which is consistent with the field test pressure.[42] Moreover, we assume that the fluids in the production well follow Darcy's law, the permeability, porosity and capillary pressure in which is 1×10^{-9} m^2 (1000 D), 1.0, and 0, respectively. For the fracture cases, a high permeability (1000 mD) zone is used to describe the hydraulic fracturing zone, without considering the detailed hydraulic fracturing method and process.[38] Before production, it is just deemed that the fractured zone has been created. As shown in Figure 1(a), the vertical section of the fractured zone is rectangular with a height of 5 m. To explore the effect of fracture depth and length on the production behavoirs of hydrate reservoir, the hydraulic fracturing is perforated at the upper, middle and lower of hydrate layers, respectively (the specific parameters can be seen in section 3.2).

In this study, the following assumptions are also made: (a) the porous medium in the reservoir is homogeneous, and the hydrate is a mono-component methane hydrate ($CH_4\cdot6H_2O$). (b) Hydrate and solid-phase sediments in the reservoir are immovable, and gas/liquid flow in porous media follows Darcy's law. (c) The dissolution of methane in the liquid phase complies with Henry's law. (d) The process of hydrate formation and dissociation is based on the phase equilibrium reaction. (e) During

hydrate dissociation, the permeability in reservoir depends on the change of fluid porosity and satisfies the Kozeny-Carman equation. (f) The fractured zone can be represented by an approximate geometric square, and the other parameters of the zone maintain the original reservoir values except the permeability.

2.3 Initial and Boundary Conditions

The initial conditions of hydrate reservoir is determined according to the process described by Moridis et al.[43,44] The top and bottom boundaries of the simulated domain (corresponding to the uppermost and lowermost grid block layers, respectively) are set as a constant pressure and temperature.[47,48] The geothermal gradient at this site is 0.0443 °C/m with a seabed temperature of 3.7 °C, and the pressure in the sediments is considered to follow the hydrostatic distribution. Then, the temperature and pressure of the boundary layers can be determined, where the pressure is calculated using the pressure, temperature and salinity-adjusted water density.[49] Finally, the actual initial conditions of each grid block are obtained through a trial and error process. The initial pressure and temperature at the bottom of hydrate layer II is 15.521 MPa, 14.93 °C, respectively. The top/bottom boundary of the domain is set as permeable that can replenish water removed within the hydrate-bearing system. A flowing boundary is assumed at the outermost of the domain, which allows fluids and heat flow through to depict a larger-scale hydrate reservoir.[40] The other parameters and conditions used in the model can be found in Table 2.

2.4 Numerical Code

In this study, MeshMaker V1.5 was used to describe the system geometry and discretize the model domain.[50] The numerical simulation results were calculated using the improved TOUGH + HYDRATE. The code includes the phase equilibrium model (used in this study) and the kinetics model of hydrate formation and dissociation. In which, the heat flow and material components (water, methane, hydrate and water-soluble inhibitors) are considered, and different components can exist in the phase of gas, liquid, ice and hydrate, so the process of hydrate dissociation under different stimulation methods can be described completely.[43] TOUGH + HYDRATE

has been widely used in the exploitation prediction of several actual gas hydrate reservoirs.

2.5 Model Validation

To accurately predict the long-term gas production of hydrate reservoir in the SHCS, a validation test was first carried out by comparing the cumulative gas production at wellhead (Q_P) of the simulated results with the field test results, as shown in Figure 2. It can be seen that in the initial 22 days, the Q_P of the simulated case is quite different from which of the actual test. This phenomenon may be due to the increase of free gas saturation and effective permeability of the reservoir near the wellbore, which is induced by the drilling operations during actual production.[50] Afterwards, the simulated results are basically consistent with the actual test results, verifying the validity of the model established in this study, and then it can be applied to subsequent calculations.

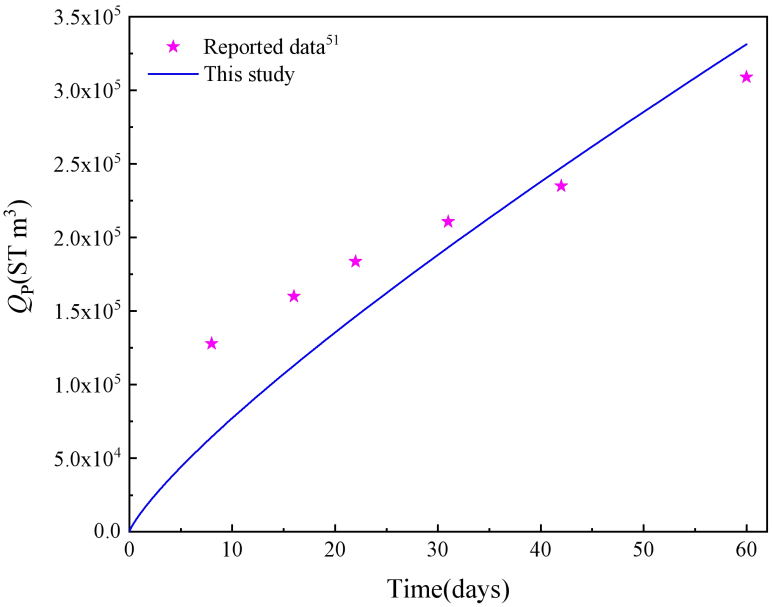

Figure 2 Comparison of Q_P in the simulated results and the field test

3. RESULTS AND DISCUSSION

3.1 Prediction of Long-term Depressurization Production of the Reservoir

Herein, a 10-year depressurization result was calculated to predict the long-term production situation of hydrate reservoir in the SHSC (case 1). The impact of underlying free gas during production was evaluated, by comparing the difference of hydrate dissociation, gas and water production in case 1 with the reservoir lacking

underlying free gas (case 2).

3.1.1 Hydrate Dissociation Behavior

Figure 3 shows the spatial distribution of pressure, temperature, hydrate saturation and gas saturation (P, T, S_H and S_G) under different production periods (60 days, 1 year, 2 years, 5 years, and 10 years). It can be seen during the initial 60 days, hydrate dissociation is mainly concentrated near the wellbore (low-temperature region caused by endothermic nature of hydrate dissociation), advancing at a uniform radial speed along with hydrate layer I, while hydrate layer II slightly lags behind layer I. A remark pressure gradient is generated near the wellbore, which is due to the rapid dissociation of hydrate, resulting in an increase of effective permeability in this area. At the same time, the undissociated hydrate region with low permeability on the right provides a barrier for pressure propagation in the reservoir. Driven by pressure difference, the free gas existing in hydrate layer II accumulates near the wellbore to cause the "Joule-Thomson" effect so that the temperature of hydrate layer II near the wellbore is lower than that of hydrate layer I. Meanwhile, the thermal fluids in the lower formation flow to the wellbore (isotherms with higher values converge near the wellbore), this is also why the dissociation rate of the lower part of hydrate layer II is significantly faster than that of the upper part. Subsequently, the hydrate dissociation front continues to expand far away, and the uppermost interface of the hydrate layer I begins to become sharp when production reaches 1 year. It is because the upper fluids with a lower temperature than hydrate layer I flow into the dissociated region driven by pressure difference and gravity, thereby hindering the hydrate dissociation. Driven by heat conduction between cold and hot fluids, the low-temperature region near wellbore gradually disappears and begins to recover.[52,53]

With the process of production, the shape of the dissociation front of hydrate layer I is gradually similar to that of hydrate layer II. Noteworthy, since the difference of phase saturations and porosity in hydrate layer I and II (especially the existence of free gas in hydrate layer II), the dissociation front presents an irregular shape near the interface between the two. Due to the existence of initial free gas contained in mud layer and hydrate layer II and the floating effect of gas itself, the hydrate saturation

near the interface of hydrate layers increases during production. Especially when production reaches 10 years, massive secondary hydrate forms and accumulates (the endothermic heat of hydrate dissociation and exothermic heat of hydrate formation offset each other, so the temperature change in the corresponding region is weak) at the bottom of the dissociation front of hydrate layer I and near the interface of hydrate layers. Correspondingly, the floating effect of gas also resulted in the accumulation of a free gas layer with higher saturation at the upper part of mud layer. Besides, it can be found there is no gas escaping or crossing over the overburden, indicating that the unproduced gas is retained or combined with free water in the sedimentary layer to reform hydrate.

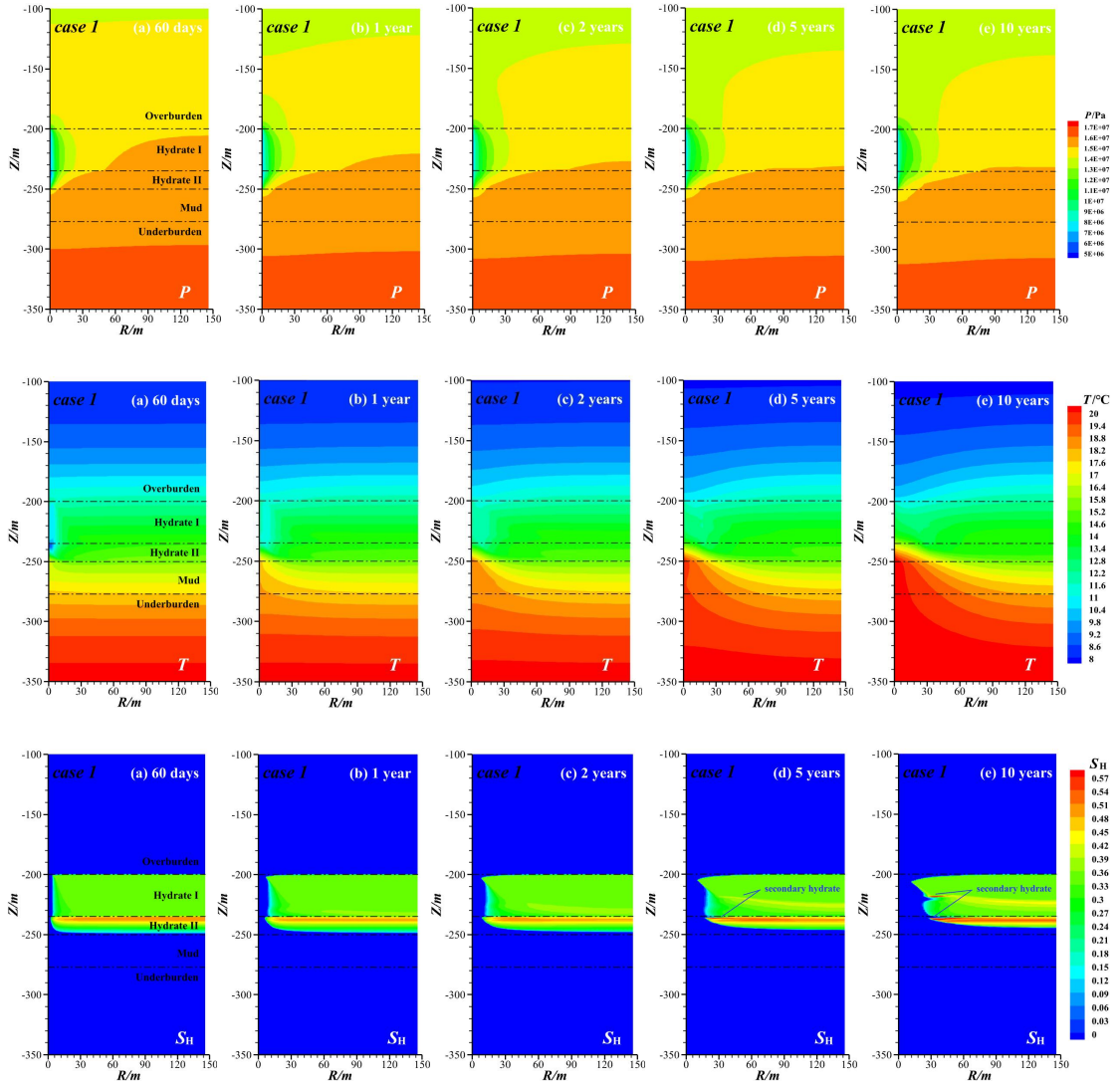

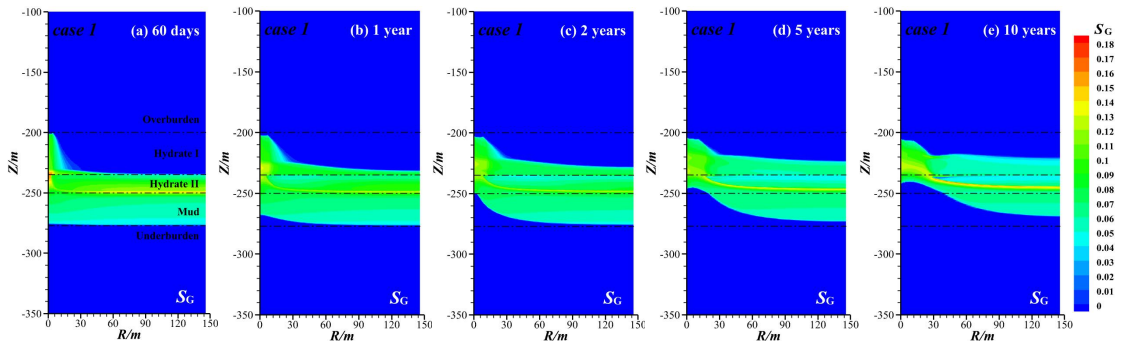

Figure 3 Evolution of spatial distribution of *P*, *T*, S_H and S_G in case 1

3.1.2 Gas and Water Production Behaviors

Figure 4 shows the variations of the volumetric rate of gas released from hydrate (V_R) and gas production at wellhead (V_P) over time, and the cumulative volume of released gas and gas production at wellhead (Q_R and Q_P) over time, respectively. It can be seen that in the initial days, V_R rapidly increases to 219,165 ST m^3/d, and V_P reaches 78,449 ST m^3/d, because the driving pressure difference (the pressure difference between the wellhead and sedimentary layer) of the fluids is the largest at this time. This is also one of the reasons for the high gas production rate in the early stage of the field test (Figure 2). Then, V_R and V_P decrease drastically. Until 30 days, Q_R (217,400 ST m^3) is far more than Q_P (190,239 ST m^3), which indicates that not all the dissociated gas flows into the wellhead and a considerable part of which is retained in the reservoir.

Subsequently, V_P and V_R continue to decrease, and the former quickly exceeds the latter. Because with the process of production, massive pore water in reservoir driven by the pressure difference between the wellbore and sedimentary layer rushes to the wellbore, hindering gas flow to the wellbore. Moreover, the lower temperature (caused by the endothermic nature of hydrate dissociation) in the dissociated region is not conducive to hydrate dissociation. It also can be seen from the spatial distribution variation of S_H in Figure 3 that, the upper dissociated region of hydrate layer I and overburden, the lower dissociated region of hydrate layer II and mud layer has been connected, respectively. In addition, the formation of secondary hydrate could affect the hydrate dissociation and wellhead gas production. When production reaches 10 years, V_R (1,282 ST m^3/d) decreases to 0.58% of the initial value, and V_P fall to 2,584

ST m^3/d, which is much less than the standards of commercial gas production (86,400~172,800 ST m^3/d).[23] As shown in Figure 4(b), the difference between Q_P and Q_R increases with the progress of production, that is, the proportion of dissociated gas in the wellhead continues to decline. During 10 years, Q_R is about 5.8 × 10^6 ST m^3, while Q_P is up to 1.0 × 10^7 ST m^3, indicating that almost half of wellhead gas production comes from the dissolved gas in seawater and the initial free gas contained in sediments.

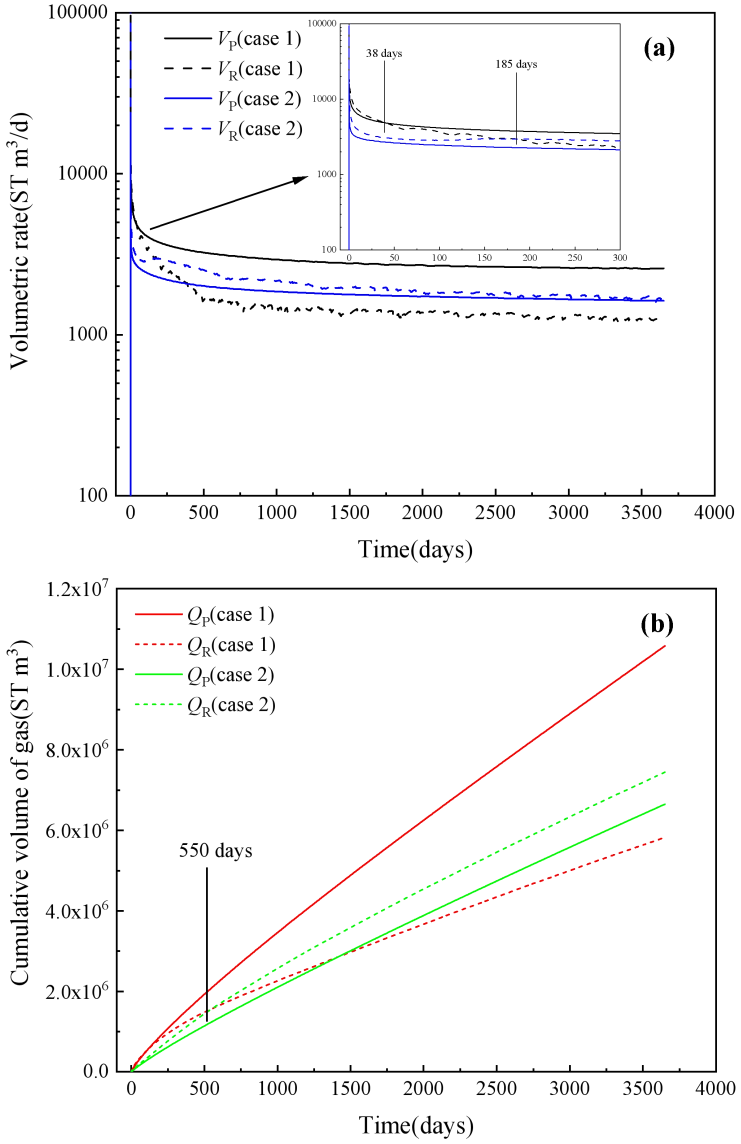

Figure 4 Variations of V_R, V_P, Q_R, and Q_P over time in case 1 and case 2

The variations of cumulative water production M_W and gas-liquid ratio R_{GW} at wellhead over time are shown in Figure 5. It can be seen that contrary to the law of gas production, the water production rate increases slowly over time, which may be

caused by the increase of effective permeability in the hydrate dissociation region. From the results of R_{GW}, it can be clearly seen the R_{GW} value is below 10 during most of the production period, indicating the exploitation economy of the reservoir under current conditions is extremely poor.

Herein, we roughly estimated the amount of water supplied to the reservoir system from outside M_S based on the law of mass conservation: $M_S = M_R + M_W - M_0 - M_D$. In which, M_R is the residual amount of water in the reservoir, M_0 is the initial total amount of water in the reservoir, and M_D is the cumulative water released from hydrate. It can be easily calculated that M_S is about 4.17×10^8 kg when the reservoir is produced for 10 years, which is about 2.64 times of M_W (1.58×10^8 kg). That is also one of the reasons for the low production efficiency of the reservoir. The former is remarkably higher than the latter, which could be related to the water consumption for the secondary hydrate formation during production.

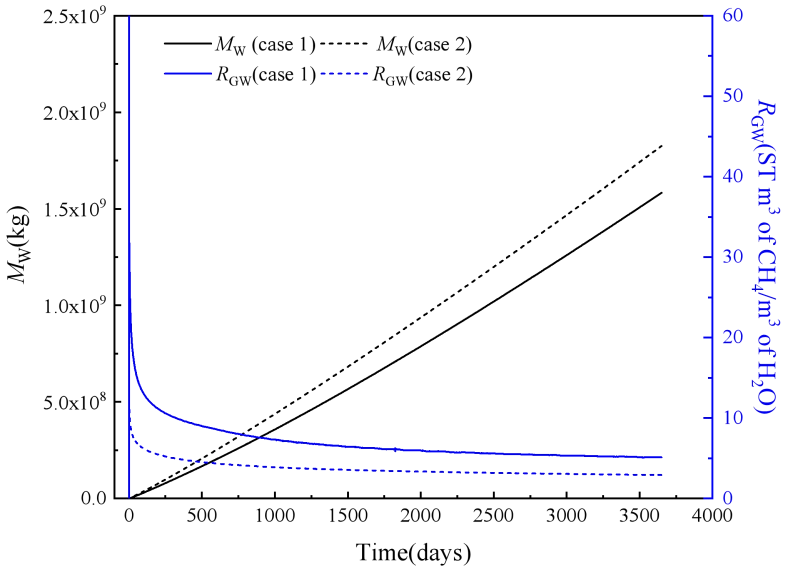

Figure 5 Variations of M_W and R_{GW} over time in case 1 and case 2

3.1.3 The Role of Underlying Free Gas During Production

Furthermore, we calculated the production results of the reservoir lacking underlying free gas (case 2) by modifying the parameters of original reservoir model. The specific modifications are as follows: the average initial hydrate saturation S_H and water saturation S_A of hydrate layer II is set as 0.31 and 0.69, respectively, and the initial water saturation S_A of the mud layer is set as 1.0. Other parameters and

formation conditions are consistent with the original model (case 1).

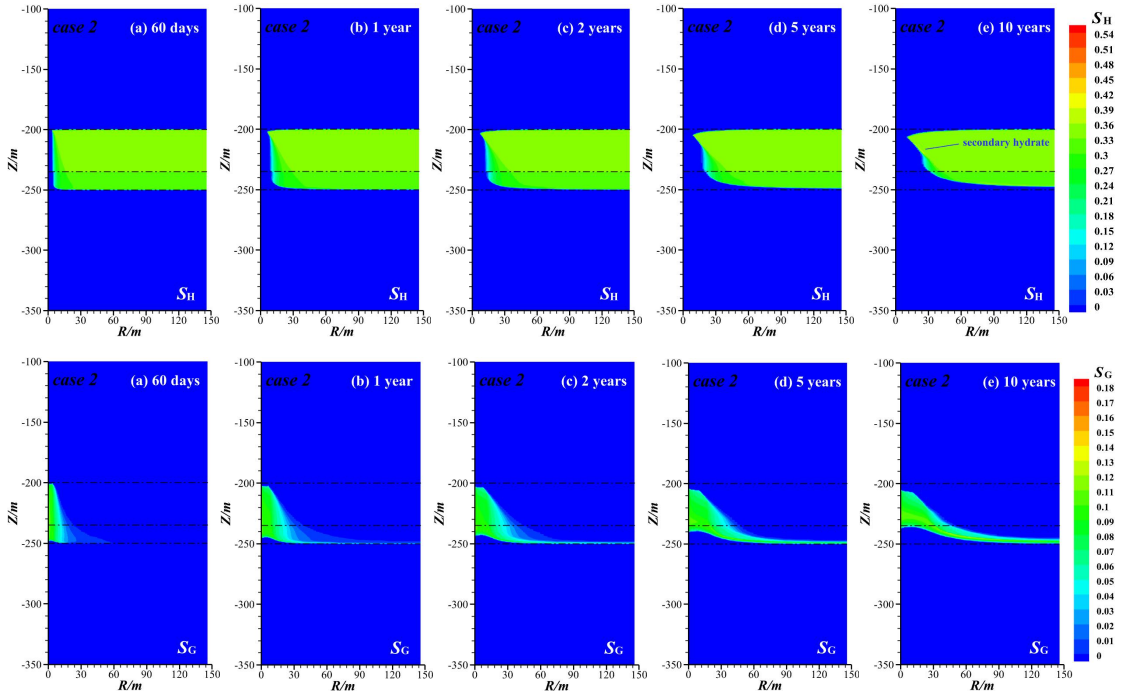

Figure 6 Evolution of spatial distribution of *P*, S_H and S_G in case 2

From the spatial distribution of S_H in Figure 6, when production to 1 year, the radial expansion of the dissociation front of hydrate layer II for case 2 is faster than that of hydrate layer I, this is different from case 1. 10 years after production, the dissociation front of hydrate layers I and II merge into a smooth interface. At this time, the amount of dissociated hydrate in case 2 accounts for about 10.46% of the total reserves, and which is higher than that in case 1 (Figure 7). That is to say, the existence of underlying free gas could be against the hydrate dissociation in the sedimentary layer. The spatial distribution of S_G shows that the gas mainly accumulates in the area between the wellbore and hydrate dissociation front, and does not appear in other layers, indicating that the gas flow is limited in the low permeability reservoir.

As shown in Figure 4(a), due to the existence of initial free gas, the V_P in case 1 is always greater than that in case 2 in early days. In the initial 185 days, the V_R of the former is higher than that of the latter, this may be because of the disturbance of free gas accumulated at the interlayer interface of hydrate layers, promoting the hydrate dissociation. Correspondingly, on the ~550th day, the Q_R in case 2 exceeds that in

case 1, because the floating of underlying free gas hinders the contact between the lower thermal fluids and the lower dissociation edge of hydrate layer II, thereby weakening the heat conduction between them. During the overall production, the Q_P in case 1 is always greater than that in case 2 (the Q_P of the former is about 59% higher than that of the latter), which is mainly due to the contribution of free gas. In addition, it can be seen from the results of water production in Figure 5, when produced to 10 years, the M_W in case 2 is about 1.82×10^9 kg, raised by ~15% compared to case 1, indicating that the existence of underlying free gas can significantly reduce the cumulative water production at wellhead. Correspondingly, the R_{GW} of the latter is always greater than that of the former. Therefore, from the perspective of wellhead water production and gas-liquid ratio, the existence of underlying free gas is conducive to the production of hydrate reservoir, this is consistent with the results of Lu et al.[30]

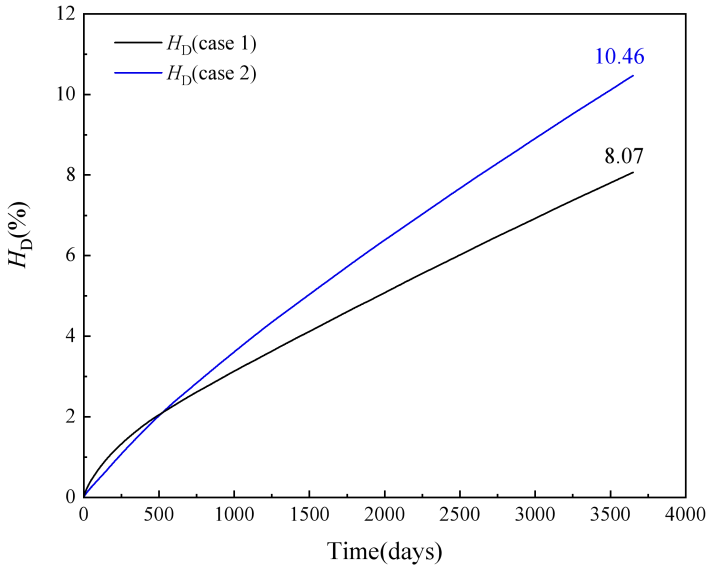

Figure 7 Percentage of hydrate dissociation in case 1 and case 2

3.2 Application of Hydraulic Fracturing

Further, we predicted the long-term production performance of the reservoir after hydraulic fracturing was performed in the partial area, and evaluated the effect of fracture depth and fracture length on the reservoir production. In subsequent statements, the reservoir with a radial length of 30 m fracture at 10 m (upper), 22 m (middle) and 35 m (lower) from the bottom of overburden, is denoted as case 3, case 4

and case 5, respectively. Similarly, when the radial length of the middle fracture is 15 m and 45 m, the reservoir is denoted as case 6 and case 7, respectively.

3.2.1 Hydrate Dissociation, Gas and Water Production Behaviors

By taking case 4 as an example, we evaluated the impact of hydraulic fracturing on reservoir production. From the distribution of P in Figure 8, the pressure radial propagation in case 4 is much faster than that in the case 1 (Figure 3), and the low-pressure region is significantly expanded due to the relatively high permeability of the fractured zone.[37] Unsurprisingly, the phase equilibrium conditions of hydrate near wellbore and in fractured zone are broken out and the hydrate dissociates first, resulting in an enlarged low-temperature region compared with the case 1. In case 4, there is still some hydrate remaining at the far end of the fractured zone due to the low temperature caused by the endothermic of hydrate dissociation. However, it is worth noting that a "binocular" shaped area of hydrate dissociation, is formed at the distal end of the fractured zone, and the area is gradually enlarged and merges each other with the progress of production. This phenomenon is mainly because that the free water with relatively high temperature from the overburden seeps into the area driven by the difference of pressure, permeability and gravity, which accelerates the dissociation of hydrate in this region.

When production reaches 5 years, the hydrate dissociation region is further expanded, and the free water from overburden and underburden converges and influxes into the wellbore, seriously hindering the flow of gas into the wellbore, which can be reflected by the extremely low inflow band of gas near wellbore (distribution of S_G). This also indicates the low production efficiency of the reservoir at this time. As production for 10 years, the hydrate dissociation region in case 4 is significantly larger than that in the case 1. At this time, the complete dissociation radius of hydrate for the former is about 36.5 m, almost 2.9 times as much as the latter, and the maximum dissociation radius of which can reach ~70 m. Correspondingly, the H_D in the reservoir for the former is about 26.89%, almost 3.3 times as much as the latter, as shown in Figure 10(c). It can be seen from Figure 10(a), the Q_P of case 4 increases by 1.59 times compared to the case 1. Unfortunately but expected, the M_W

also be doubled accordingly, as shown in Figure 10(b). That is to say, the application of hydraulic fracturing is helpful for hydrate dissociation and gas production at wellhead, yet could no obvious advantage in improving production efficiency, which also can be seen from the results of R_{GW} in Figure 10(d).

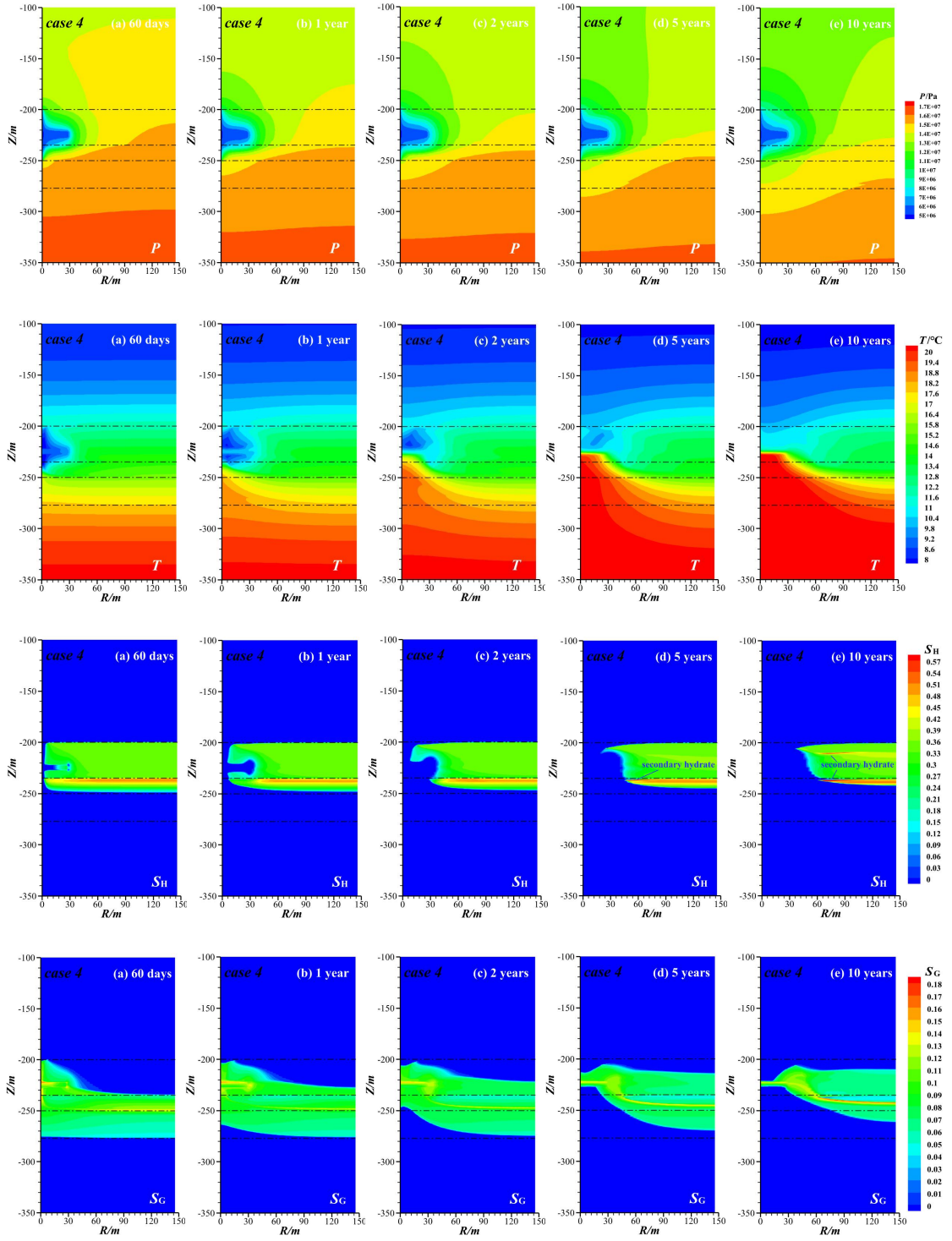

Figure 8 Evolution of spatial distribution of *P*, *T*, S_H and S_G in case 4

3.2.2 Effect of Fracture Depth

For the hydrate reservoir with a certain thickness fracture, the different fracture depths will also affect the hydrate dissociation and gas production in the reservoir. So we evaluated the production performance of the hydrate reservoir when the fractured zone is located at the upper (case 3), middle (case 4) and lower (case 5) part of the hydrate layers, where the hydrate layer I and II is regarded as an integral layer.

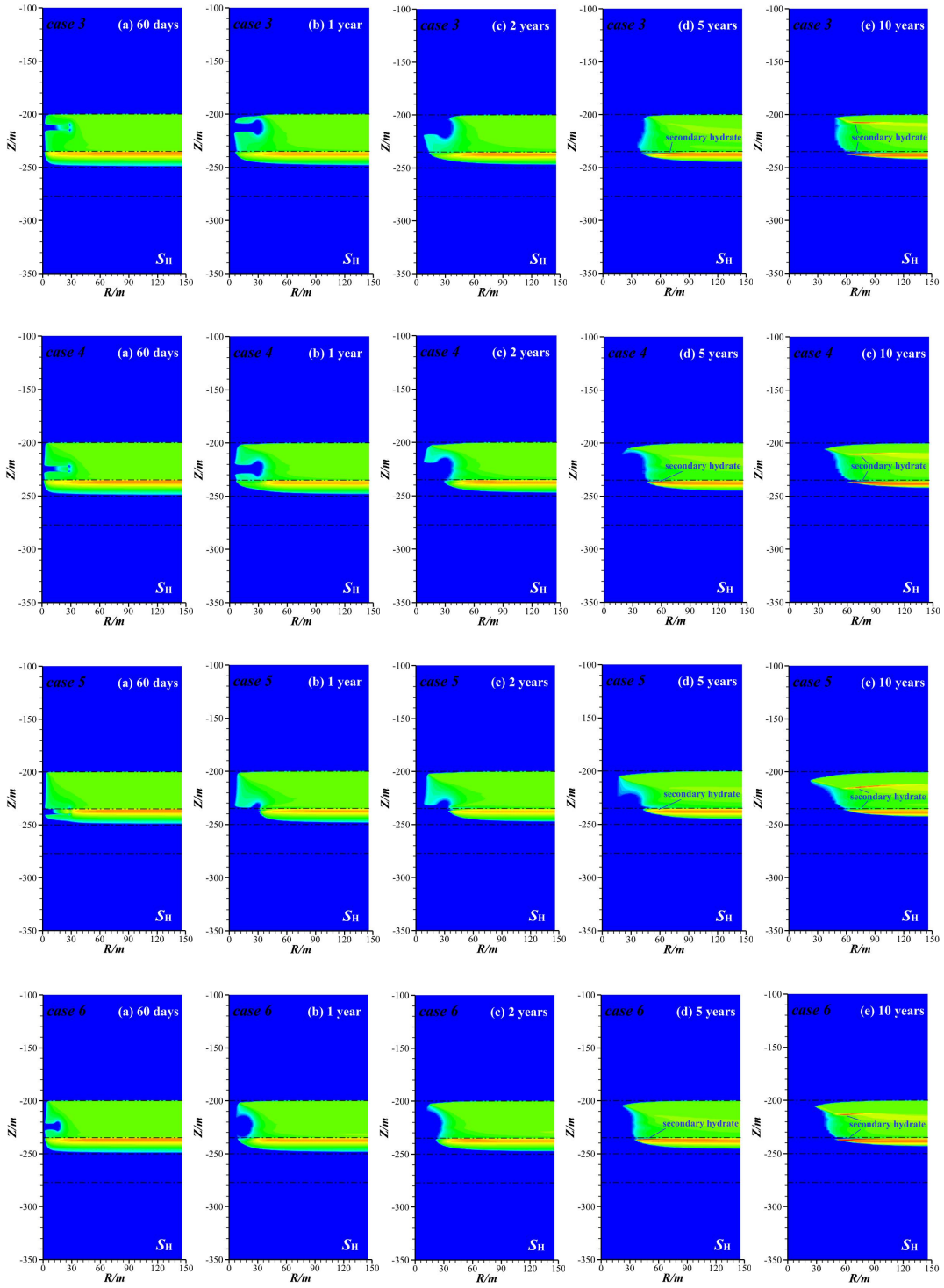

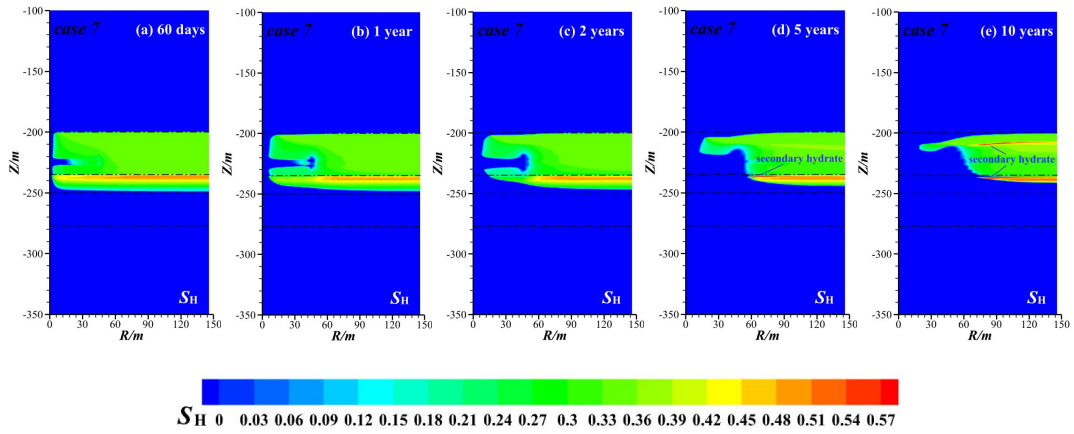

Figure 9 Evolution of spatial distribution of S_H in case 3 to 7

As shown in Figure 9, the hydrate dissociation region is significantly dominated by the fracture depth, and the hydrate dissociation law over procudtion time for case 3, case 4 and case 5 is roughly similar. The difference for the three cases is the precedence of the hydrate dissociation region, which also affects the capacity of production at wellhead. In case 3, the hydrate near the upper of the integral layer speedily dissociates and then the dissociated region is connected with the overburden, resulting in massive water pours into the wellbore driven by gravity and pressure difference, which hinders the output of dissociated gas. Similarly, in case 5, the hydrate near the lower of the integral layer rapidly dissociates and the dissociated region is connected with the mud layer, causing a considerable pore water contained in adjacent layers influx into the wellbore. This is also the main reason that the variation of Q_P in case 3 and case 5 is basically similar, and always lower than that in case 4, as shown in Figure 10(a). Correspondingly, the M_W in case 5 is the highest of the three, as shown in Figure 10(b), this may be also related to the relatively high intrinsic permeability of the mud layer. By comparison, in case 4, there is adequate hydrate near the fractured zone with relatively lower pressure and higher permeability, to release gas and then flow into the wellbore. Therefore, its cumulative amount of hydrate dissociation in the reservoir is the most of the three cases, as shown in Figure 10(c).

From Figure 10(d), it can be seen that all three cases can improve the R_{GW} in early days compared to the case 1. Among these, the duration time (above the case 1)

of R_{GW} for case 4 is longer than that for case 3 and case 5. Because for the latter two cases, the hydrate near the fractured zone dissociates and the area is connected with the adjacent water-rich layers prior to case 4, causing a large influx of free water into the wellbore. This is also the reason that the R_{GW} for the three cases subsequently decreases to below the case 1. All in all, whether in terms of Q_P and R_{GW}, or H_D in the reservoir, hydraulic fracturing implemented in the middle part of the integral layer is the best.

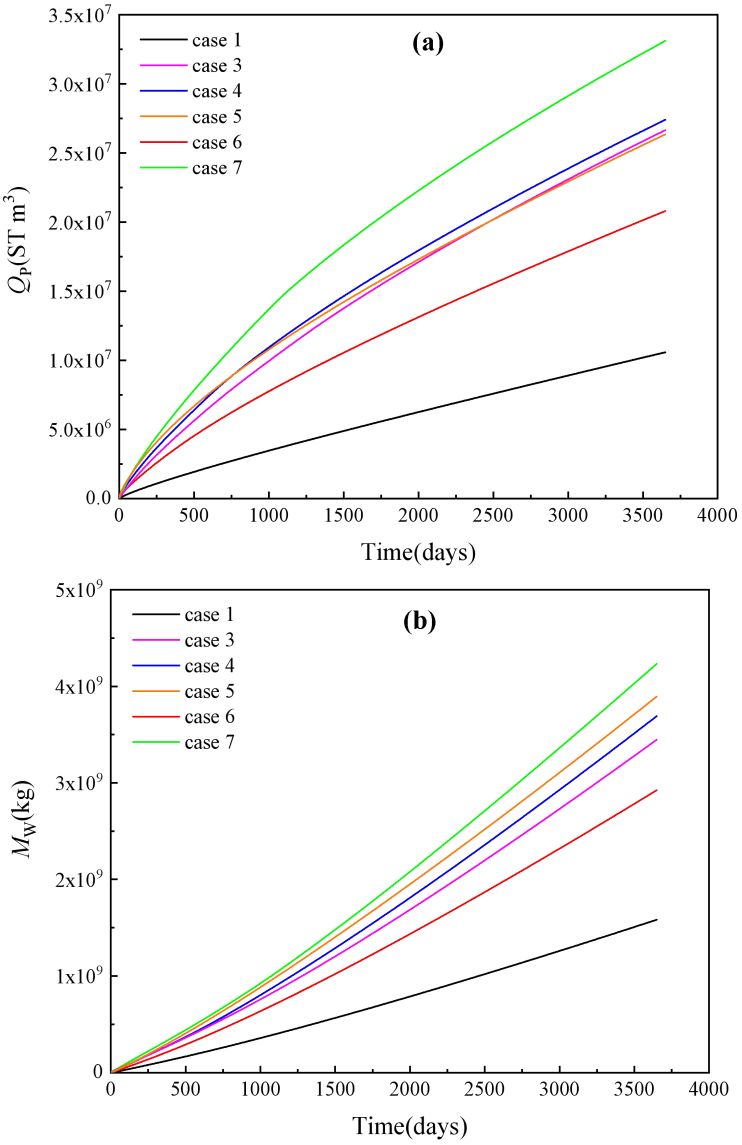

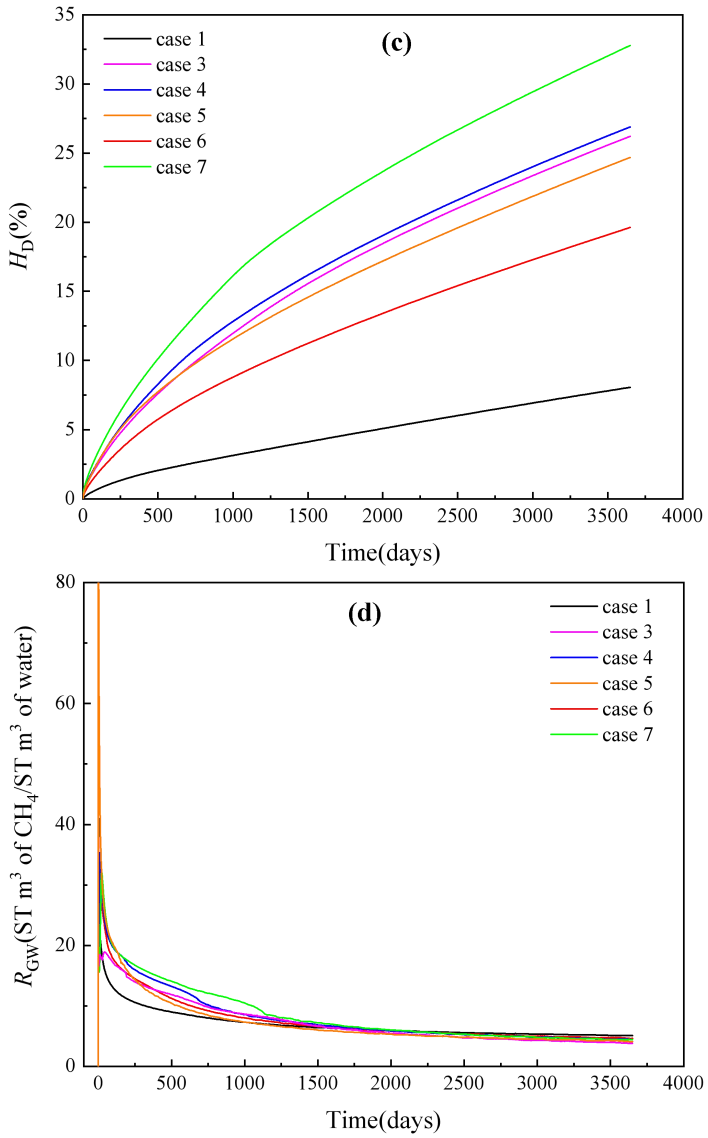

Figure 10 Variations of R_{GW} over time in different cases

3.2.3 Effect of Fracture Length

Furtherly, we evaluated the production performance of hydrate reservoir when the fractured zone with lengths of 15 m (case 6), 30 m (case 4) and 45 m (case 7), respectively, is located in the middle part of the integral layer. As shown in Figure 9, with the expansion of fracture length, the hydrate dissociation region enlarges. Correspondingly, Q_P, M_W, the duration time of R_{GW}, and H_D remarkably increase (Figure 10). Interestingly, the longitudinal area of hydrate dissociation near the fractured zone gradually narrows with the fracture length increasing from 15 m to 45 m. It is mainly because the endothermic of hydrate dissociation leads to the formation of a low-temperature region along the fractured zone, and the heat absorption capacity

is directly proportional to the amount of hydrate dissociation, resulting in a slow temperature recovery rate for the case with a long fracture length. Especially in case 7, when production reaches 5 years, there is still a tail-shaped hydrate residue region between the upper part of hydrate layer I and the fractured zone, due to the cooling effect of low-temperature fluids from the overburden. These phenomena indicate that the timeliness of heat conduction between the hydrate undissociated region and surrounding environments is very critical during production. For all cases, it is obvious that a large number of secondary hydrate forms and gathers near the bottom of the dissociation front of hydrate layer I and the interface of two hydrate layers, which is also an important problem in the future production of hydrate reservoir.

3.2.4 Positive and Negative Impacts of Hydraulic Fracturing

To clearly understand the enhancing effect of hydraulic fracturing on the production of hydrate reservoir, we also compared the radial distance of dissociation front (R_D) at the middle planes of the fractured zone under different production times (60 days, 1 year, 2 years, 5 years and 10 years), as shown in Figure 11. For all cases, the R_D increases over time. Compared with the case 1, the R_D for the fracture cases significantly increase, especially for case 7. Figure 12 shows the radial distribution of pressure and temperature along the middle plane of the fractured zone in case 7 when production for 10 years. It can be seen that the pressures in case 7 are always lower than those in the case 1, indicating that hydraulic fracturing can obviously promote pressure propagation in the sediments, and is conducive to hydrate dissociation. As expected, an inflection point occurs at 63 m, which is near the hydrate dissocaition front. Correspondingly, the temperatures in case 7 are higher than those in case 1 within the first 40 m (close to the fracture length), due to the invasion of underlying thermal fluids into the hydrate dissociated region. Then the temperature rapidly drops below the temperature in the case 1. In the two cases, it can be noted that the lowest temperatures all occur near the dissociation front.

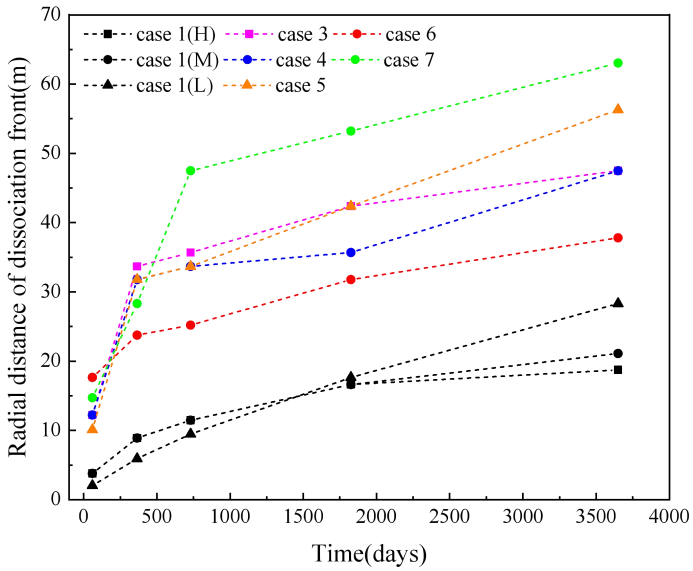

Figure 11 Variations of R_D at the middle planes of fractured zone over time in different cases

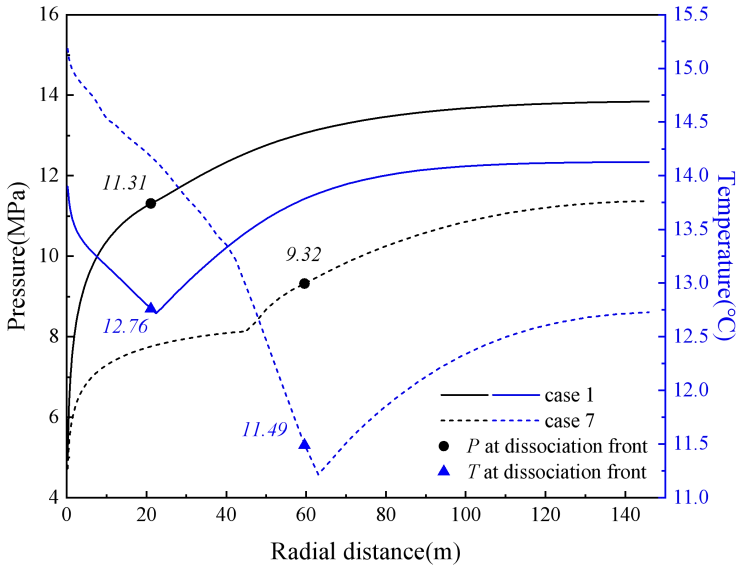

Figure 12 *P* and *T* along the middle plane of fractured zone in case 7 at 10 years

In addition, the implementation of hydraulic fracturing could also bring some potential negative effects on hydrate reservoir production, and a key issue is the massive output of water. From Figure 13, it can be seen that the gas active area near wellbore, especially in case 7, decreases with the process of production, which is closely related to the difference of pressure, gas/liquid permeability, and saturation, etc. Furthermore, we roughly compared the proportion of gas/water active area near wellbore in different cases when produced to 10 years, as shown in Figure 14. Unfortunately, compared with the original reservoir (case 1), the proportion of gas active area in all fractured reservoirs is reduced to varying degrees, this indicates that

the water production rate at wellhead is huge at this time. There is no doubt that in the early stage, the implementation of hydraulic fracturing can accelerate the hydrate dissociation and gas production in reservoir. Once the hydrate near the fractured zone is exhausted, the high permeability in this zone also provides a convenient channel for the water flow in sedimentary layer. After the implementation of hydraulic fracturing, more overlying/underlying water could be involved due to the further propagation of pressure in reservoir (can be seen in Figure 8). In the actual reservoir, the flow of a large amount of water will ineviably promote the migration of sand in the sedimentary layer, increase the risk of wellhead sand production, and affect the safety production of the reservoir. This is contrary to the original intention (more gas, less water and sand are produced) of hydrate reservoir production. That is to say, only through the implementation of hydraulic fracturing without other auxiliary means, the exploitation economy of the hydrate reservoir is still poor.

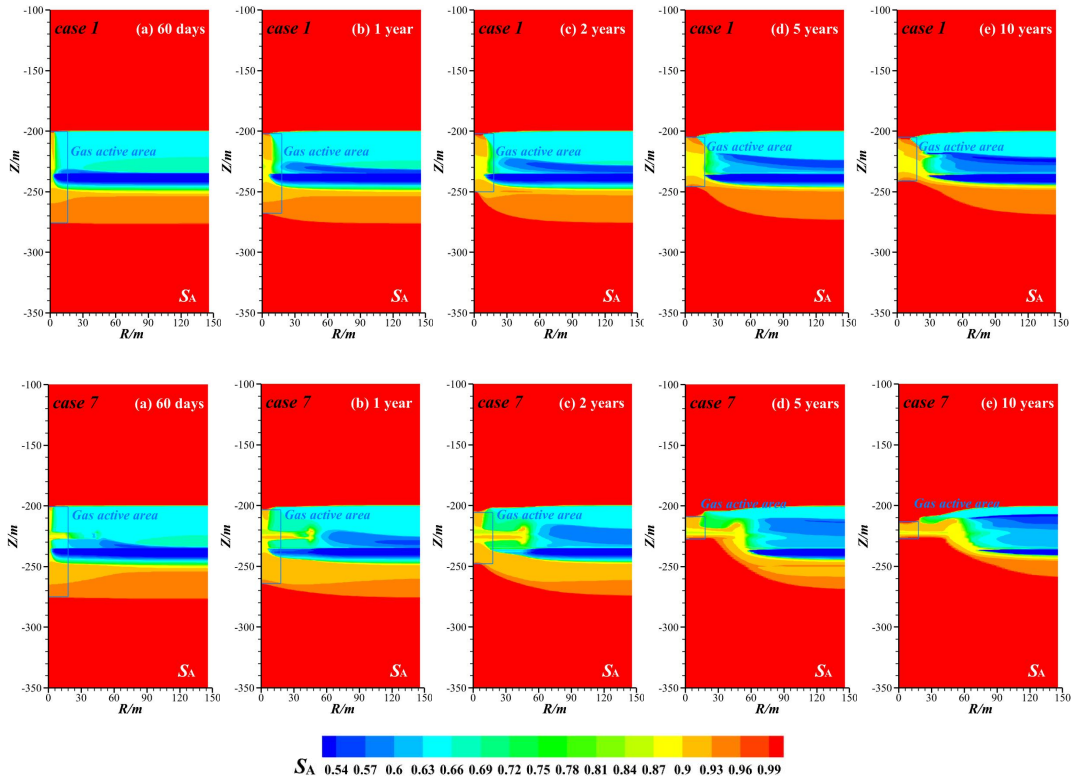

Figure 13 Evolution of Spatial distribution of S_A in case 1 and case 7

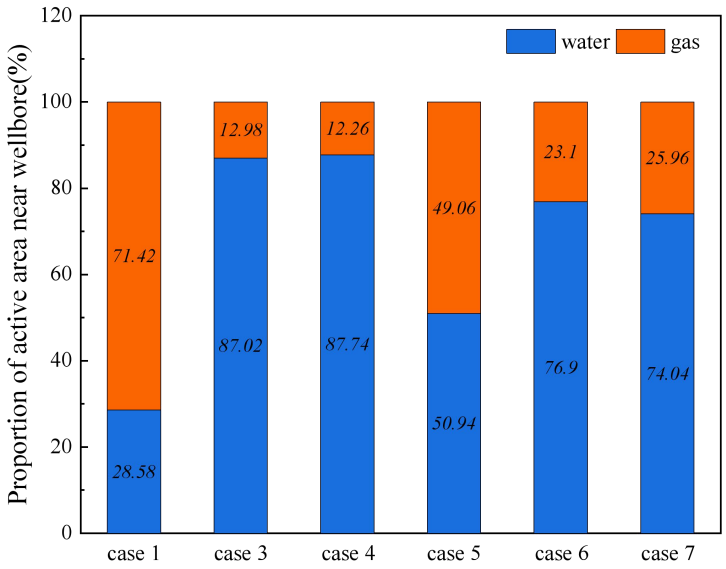

Figure 14 Proportion of gas/water active area near wellbore in different cases at 10 years

4. CONCLUSIONS

In this study, we predicted the production performance of multilayer hydrate reservoir during a long-term depressurization, evaluated the impacts of underlying free gas and application of hydraulic fracturing on hydrate dissociation, gas and water production behaviors in the reservoir. The main conclusions can be drawn as follows:

(1) In the early days, the endothermic nature of hydrate dissociation and the "Joule-Thomson" effect caused by the free gas influx into the wellbore, leading to a low-temperature region near wellbore. As production progresses, the hydrate dissociation decelerates. Once the hydrate dissociation region is compatible and connected with the adjacent layers, the free water in sedimentary layers will flow into the wellbore driven by pressure difference or gravity, hindering the production of gas. During production, the timeliness of heat conduction between the hydrate layers and surrounding environments is very critical, which will significantly affect the hydrate dissociation.

(2) Almost half of the produced gas comes from dissolved gas in pore water and free gas in the sedimentary layer itself, and there is no gas escaping through the overburden. A large part of dissociated gas is remained or combined with free water in the reservoir to reform hydrate. Massive secondary hydrate forms and gathers near the bottom of the dissociation front of hydrate layer I and the

interface of hydrate layers. From the perspective of gas production, water production and gas-liquid ratio at wellhead, the existence of underlying free gas is conducive to hydrate reservoir production.

(3) The application of hydraulic fracturing can remarkably promote the hydrate dissociation and improve wellhead gas production, especially when a long-distance fracture is performed in the middle part of hydrate layer. After hydraulic fracturing, the gas-liquid ratio of reservoir production, can be improved in the early days, and more overlying/underlying water could be involved. Only through the implementation of fracturing without other auxiliary means, the depressurization production of hydrate reservoir is not sufficient to meet the standards of commercial exploitation.

AUTHOR INFORMATION

Corresponding Author

Tao Lv-*College of Petroleum Engineering, Xi'an Shiyou University, Xi'an 710065, PR China*; orcid.org/0000-0003-4926-2565; E-mail: lvtao@xsyu.edu.cn

Notes

The authors declare that they have no known competing financial interests or personal relationships that could have appeared to influence the work reported in this paper.

ACKNOWLEDGMENTS

This work is supported by the Key Laboratory of Gas Hydrate, Guangzhou Institute of Energy Conversion, Chinese Academy of Sciences (No. E129kf1501), the National Natural Science Foundation of China (51576202 and 51736009), and the Guangdong Major project of Basic and Applied Basic Research (No.2020B0301030003).

REFERENCES

[1] Mao, W.L.; Mao, H.K.; Goncharov, A.F.; Struzhkin, W.; Guo, Q.; Hu, J.; Shu, J.; Hemley, R.J.; Somayazulu, M.; Zhao, Y. Hydrogen clusters in clathrate hydrate. *Science* **2002**, 297, 2247-2249.

[2] Moridis, G.J.; Collett, T.S.; Pooladi-Darvish, M.; Hancock, S.H.; Santamarina, J.C.; Boswell, R.; Kneafsey, T.; Rutqvist, J.; Kowalsky, M.B.; Reagan, M.T.; Sloan, E.D.; Sum, A.K.; Koh, C.A. Challenges, uncertainties and issues facing gas production from gas-hydrate deposits. *SPE Reservoir Eval. Eng*. **2011**, 14, 76-112.

[3] Makogon, Y.F.; Holditch, S.A.; Makogon, T.F. Natural gas hydrates-a potential energy source for the 21st Century. *J. Petrol. Sci. Eng*. **2007**, 56, 14-31.

[4] Chong, Z.R.; Yang, S.H.B.; Babu, P.; Linga, P.; Li, X.S. Review of natural gas hydrates as an energy resource: Prospects and challenges. *Appl. Energy*. **2016**, 162, 1633-1652.

[5] Moridis, G.J.; Silpngarmlert, S.; Reagan, M.T.; Collett, T.; Zhang, K. Gas production from a cold, stratigraphically-bounded gas hydrate deposit at the Mount Elbert gas hydrate stratigraphic test well, Alaska North Slope: implications of uncertainties. *Mar. Pet. Geol*. **2011**, 28, 517-534.

[6] Konno, Y.; Masuda, Y.; Hariguchi, Y.; Kurihara, M.; Ouchi, H. Key factors for depressurization-induced gas production from oceanic methane hydrates. *Energy Fuels* **2010**, 24, 1736-1744.

[7] Li, G.; Moridis, G.J.; Zhang, K.N.; Li, X.S. The use of huff and puff method in a single horizontal well in gas production from marine gas hydrate deposits in the Shenhu Area of South China Sea. *J. Petrol. Sci. Eng*. **2011**, 77, 49-68.

[8] Chen, Z.Y.; Feng J.C.; Li, X.S.; Zhang, Y.; Li, B.; Lv, Q.N. Preparation of warm brine in situ seafloor based on the hydrate process for marine gas hydrate thermal stimulation. *Ind. Eng. Chem. Res*. **2014**, 53, 14142-14157.

[9] Ohgaki, K.; Takano, K.; Sangawa, H.; Matsubara, T.; Shinya, Nakano, S. Methane exploitation by carbon dioxide from gas hydrates-phase equilibria for CO_2-CH_4 mixed hydrate system. *J. Chem. Eng. Jpn*. **1996**, 29, 478-483.

[10] Kawamura, T.; Sakamoto, Y.; Ohtake, M.; Yamamoto, Y.; Haneda, H.; Komai, T. Dissociation behavior of hydrate core sample using thermodynamic inhibitor-part 2: experimental investigation using long core samples. *Int. J. Offshore. Polar*. **2008**, 18, 156-159.

[11] Feng, J.C.; Li, B.; Li, X.S.; Wang, Y. Effects of depressurizing rate on methane hydrate dissociation within large-scale experimental simulator. *Appl. Energ*. **2021**, 304, 117750.

[12] Li, X.S.; Zhang, Y.; Li, G.; Chen, Z.Y.; Wu, H.J. Experimental investigation into the production behavior of methane hydrate in porous sediment by depressurization with a novel three-dimensional cubic hydrate simulator. *Energy Fuels* **2011**, 25, 4497-4505.

[13] Ubeyd, B.M.; Merey, U. Gas production from methane hydrate reservoirs in different well configurations: a case study in the conditions of the Black Sea. *Energy Fuels* **2021**, 35, 1281-1296.

[14] Liu, C.L.; Li, Y.L.; Sun, J.Y.; Wu, N.Y. Gas hydrate production tests: from experimental simulation to field practice. *Marine Geology & Quaternary Geology (in Chinese)* **2017**, 37, 12-21.

[15] Phillips, S.C.; Flemings, P.B.; You, K.; Meyer, D.W.; Dong, T. Investigation of in situ salinity and methane hydrate dissociation in coarse-grained sediments by slow, stepwise depressurization. *Mar. Petrol. Geol*. **2019**, 109, 128-144.

[16] Lv, T.; Li, X.S.; Chen, Z.Y.; Sun, D.; Zhang, Y.; Yan, K.F.; Cai, J. Experimental investigation on the production behaviors of methane hydrate in sandy sediments by different depressurization strategies. *Energy Technology* **2018**, 6, 2501-2511.

[17] Gao, Q.; Yin, Z.Y.; Zhao, J.Z.; Yang, D.; Linga, P. Tuning the fluid production behaviour of hydrate-bearing sediments by multi-stage depressurization. *Chem. Eng. J*. **2021**, 406, 127174.

[18] Zhao, J.F.; Liu, Y.L.; Guo, X.W.; Wei, R.P.; Yu, T.B.; Xu, L.; Sun, L.J.; Yang, L. Gas production behavior from hydrate-bearing fine natural sediments through optimized step-wise depressurization. *Appl. Energ*. **2020**, 260, 114275.

[19] Konno, Y.; Masuda, Y.; Akamine, K.; Naiki, M.; Nagao, J. Sustainable gas production from methane hydrate reservoirs by the cyclic depressurization method. *Energ. Convers. Manage*. **2016**, 108, 439-445.

[20] Mao, P.X.; Sun, J.X.; Ning, F.L.; Chen, L.; Wan, Y.Z.; Hu, G.W.; Wu, N.Y. Numerical simulation on gas production from inclined layered methane hydrate reservoirs in the Nankai Trough: a case study. *Energy Reports* **2021**, 7, 8608-8623.

[21] Terzariol, M.; Santamarina, J.C. Multi-well strategy for gas production by depressurization from methane hydrate-bearing sediments. *Energy* **2020**, 220, 119710.

[22] Chen, Z.Y.; You, C.Y.; Lv, T.; Li, X.S.; Zhang, Y.; Xu, L.X. Numerical simulation of the depressurization production of natural gas hydrate reservoirs by vertical well patterns in the northern South China Sea. *Natural Gas Industry (in Chinese)* **2020**, 40, 177-184.

[23] Wu, N.Y.; Huang, L.; Hu, G.W.; Li, Y.L.; Chen, Q.; Liu, C.L. Geological controlling factors and scientific challenges for offshore gas hydrate exploitation. *Marine Geology & Quaternary Geology (in Chinese)* **2017**, 37, 1-11.

[24] Ye, J.L.; Qin, X.W.; Xie, W.W.; Lu, H.L.; Ma, B.J.; Qiu, H.J.; Liang, J.Q.; Lu, J.A.; Kuang, Z.G.; Lu, C.; Liang, Q.Y.; Wei, S.P.; Yu, Y.J.; Liu, C.S.; Li, B.; Shen, K.X.; Shi, H.X.; Lu, Q.P.; Li, J.; Kou, B.B.; Song, G.; Li, B.; Zhang, H.E.; Lu, H.F.; Ma, C.; Dong, Y.F.; Bian, H. Main progress of the second gas hydrate trial production in the South China Sea. *China Geology (in Chinese)* **2020**, 47, 557-568.

[25] Qin, X.W.; Lu, J.A.; Lu, H.L.; Qiu, H.J.; Liang, Q.Q.; Kang, D.J.; Zhan, L.S.; Lu, H.F.; Kuang, Z.G. Coexistence of natural gas hydrate, free gas and water in the gas hydrate system in the Shenhu Area, South China Sea. *China Geology (in Chinese)* **2020**, 3, 210-220.

[26] Kret, K.; Tsuji, T.; Chhun, C.; Takano, O. Distributions of gas hydrate and free gas accumulations associated with upward fluid flow in the Sanriku-oki Forearc Basin, Northeast Japan. *Mar. Petrol. Geol*. **2020**, 116, 104305.

[27] Mishra, C.K.; Dewangan, P.; Mukhopadhyay, R.; Banerjee. D. Velocity modeling and attribute analysis to understand the gas hydrates and free gas system in the Mannar Basin, India. *J. Nat. Gas. Sci. Eng*. **2021**, 92, 104007.
[28] Kroeger, K.F.; Crutchley, G.J.; Hillman, J.I.; Turco, F.; Barnes, P.M. Gas hydrate formation beneath thrust ridges: A test of concepts using 3D modelling at the southern Hikurangi Margin, New Zealand. *Mar. Petrol. Geol*. **2022**, 135, 105394.
[29] Zhao, J.; Zheng, J.N.; Dong, S.; Yang, M.J.; Song. Y.C. Gas production enhancement effect of underlying gas on methane hydrates in marine sediments by depressurization. *Fuel* **2022**, 310, 122415.
[30] Shang, S.L.; Gu, L.J.; Zhan, L.S.; Qiu, H.J.; Lu, H.L. Application of horizontal well to gas production from a hydrate reservoir with free gas and high irreducible water. *J. Nat. Gas. Sci. Eng*. **2021**, 94, 104102.
[31] Boswell, R.; Collett, T.S. Current perspectives on gas hydrate resources. Energy. *Environ. Sci*. **2011**, 4, 1206-1215.
[32] Zhang, L.X.; Dong, H.S.; Dai, S.; Kuang, Y.M.; Yang, L.; Wang, J.Q.; Zhao, J.F.; Song, Y.C. Effects of depressurization on gas production and water performance from excess-gas and excess-water methane hydrate accumulations. *Chem. Eng. J*. **2022**, 431, 133223.
[33] Wu, N.Y.; Li, Y.L.; Wan, Y.Z.; Sun, J.Y.; Huang, L.; Mao, P.X. Prospect of marine natural gas hydrate stimulation theory and technology system. *Natural Gas Industry (in Chinese*) **2020**, 40, 100-110.
[34] Mou, P.W.; Pan, J.N.; Wang, K.; Wei, J.; Yang, Y.H.; Wang, X.L. Influences of hydraulic fracturing on microfractures of high-rank coal under different in-situ stress conditions. *Fuel* **2020**, 287, 119566.
[35] Too, J.L.; Cheng, A.; Khoo, B.C.; Palmer, A.; Linga, P. Hydraulic fracturing in a pennyshaped fractured. Part II: Testing the frackability of methane hydrate-bearing sand. *J. Nat. Gas. Sci. Eng*. **2018**, 52, 619-628.
[36] Liu, X.Q.; Zhang, W.D.; Qu, Z.Q.; Guo, T.K.; Sun, Y.; Rabiei, M.; Cao, Q.Y. Feasibility evaluation of hydraulic fracturing in hydrate-bearing sediments based on analytic hierarchy process-entropy method (AHP-EM). *J. Nat. Gas. Sci. Eng*. **2020**, 81, 103434.
[37] Zhao, J.F.; Xu, L.; Guo, X.W.; Li, Q.P.; Lv, X.; Fan, Q.; Zhao, J.; Dong, H.S.; Wang, B.; Yang, L. Enhancing the gas production efficiency of depressurization-induced methane hydrate exploitation via fracturing. *Fuel* **2020**, 288, 119740.
[38] Feng, Y.C.; Chen, L.; Suzuki, A.; Kogawa, T.; Okajima, J.; Komiya, A.; Maruyama, S. Enhancement of gas production from methane hydrate reservoirs by the combination of hydraulic fracturing and depressurization method. *Energ. Convers. Manage*. **2019**, 184, 194-204.
[39] Ma, X.L.; Sun, Y.H.; Guo, W.; Jia, R.; Li, B. Numerical simulation of horizontal well hydraulic fracturing technology for gas production from hydrate reservoir. *Appl. Ocean. Res*. **2021**, 112, 102674.
[40] Zhang, J.M.; Li, X.S.; Chen, Z.Y.; Li, Q.P.; Li, G.; Lv, T. Numerical simulation of the improved gas production from low permeability hydrate reservoirs by

using an enlarged highly permeable well wall. *J. Petrol. Sci. Eng*. **2019**, 183, 106404.

[41] Hu, G.W.; Li, Y.L.; Wu, N.Y.; Chen, Q.; Liu, C.L.; Liu, Z.W. Undrained shear strength estimation of the cover layer of hydrate at site W18/19 of Shenhu Area. *Marine Geology & Quaternary Geology (in Chinese)* **2017**, 37, 151-157.

[42] Li, J.F.; Ye, J.L.; Qin, X.W.; Qiu, H.J.; Wu, N.Y.; Lu, H.L.; Xie, W.W.; Lu, J.A.; Peng, F.; Xu, Z.Q.; Lu, C.; Kuang, Z.G.; Wei, J.G.; Liang, Q.Y.; Lu, H.F.; Kou, B.B. The first offshore natural gas hydrate production test in South China Sea. *China Geology* **2018**, 1, 5-16.

[43] Moridis, G.J.; Kowalsky, M.B.; Pruess, K. TOUGH+HYDRATE v1.1 user's manual: a code for the simulation of system behavior in hydrate-bearing. Geologic Media, Berkeley, California, **2009**.

[44] Moridis, G.J.; Kim, J.; Reagan, M.T.; Kim, S.J. Feasibility of gas production from a gas hydrate accumulation at the UBGH2-6 site of the Ulleung basin in the Korean East Sea. *J. Petrol. Sci. Eng*. **2013**, 108, 180-210.

[45] Genuchten, M.T.V. A closed-form equation for predicting the hydraulic conductivity of unsaturated soils. *Soil. Sci. Soc. Am. J*. **1980**, 44, 892-898.

[46] Stone, H.L. Estimation of three-phase relative permeability and residual oil data. *J. Can. Pet. Technol*. **1973**, 12, 53-61.

[47] Mao, P.X.; Wu, N.Y.; Sun, J.X.; Ning, F.L.; Chen, L.; Wan, Y.Z.; Hu, G.W.; Gao, X.X. Numerical simulations of depressurization-induced gas production from hydrate reservoirs at site GMGS3-W19 with different free gas saturations in the northern south china sea. *Energy. Sci. Eng.* **2021**, 00, 1-24.

[48] Chen, C.; Meng, Y.L.; Zhong, X.P.; Nie, S.S.; Ma, Y.R.; Pan, D.B.; Liu, K.Y.; Li, X.T.; Gao, S. Research on the influence of injection-production parameters on challenging natural gas hydrate exploitation using depressurization combined with thermal injection stimulated by hydraulic fracturing. *Energy Fuels* **2021**, 35, 15589-15606.

[49] Moridis, G.J.; Reagan, M.T.; Queiruga, A.F,; Boswell, R. (2019). Evaluation of the performance of the oceanic hydrate accumulation at site NGHP-02-09 in the Krishna-Godavari basin during a production test and during single and multi-well production scenarios. *Mar. Petrol. Geol*. **2019**, 108, 660-696.

[50] Moridis, G.J. User's manual of the MeshMaker V1.5 code: a mesh generator for domain discretization in simulations of the TOUGH+ and TOUGH2 families of codes. Geologic Media, Berkeley, California, **2016**.

[51] Chen, L.; Feng, Y.C.; Okajima, J.; Komiya, A.; Maruyama, S. Production behavior and numerical analysis for 2017 methane hydrate extraction test of Shenhu, South China Sea. *J. Nat. Gas. Sci. Eng*. **2018**, 53, 55-66.

[52] Chong, Z.R.; Moh, J.W.R.; Yin, Z.Y.; Zhao, J.Z.; Linga, P. Effect of vertical wellbore incorporation on energy recovery from aqueous rich hydrate sediments. *Appl. Energ*. **2018**, 229(1), 637-647.

[53] Gao, Q.; Zhao, J.Z.; Yin, Z.Y.; Yang, D.; Zhang, C. Experimental study on fluid production from methane hydrate sediments under the marine triaxial condition. *Energy Fuels*, **2021**, 35(5), 3915-3924.

TOC Graphic

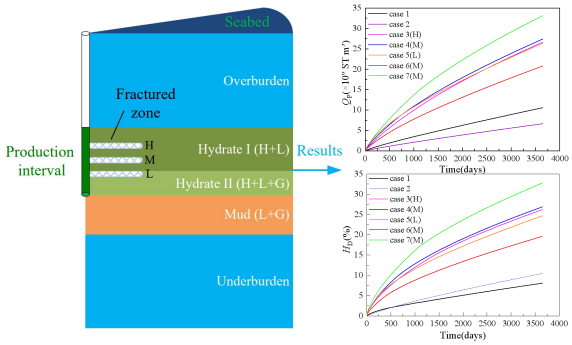
Seabed
Overburden
Fractured zone
Production interval
H
M
L
Hydrate I (H+L)
Hydrate II (H+L+G)
Mud (L+G)
Underburden
Results
case 1
case 2
case 3(H)
case 4(M)
case 5(L)
case 6(M)
case 7(M)
Time(days)